Stability-based planning and trajectory tracking of a mobile manipulator over uneven terrains

Jae-Yun Jun, Vincent Padois and Faïz Benamar

***Abstract*— The problem of improving the stability of a mobile manipulator over a sloped terrain is addressed in the present work. Such an improvement is achieved by finding the location of center of mass of the manipulator that maximizes the overall quasi-static stability defined as the force-angle stability using a stochastic optimization approach known as the Covariance Matrix Adaptation. The tracking of both trajectories for the robot base and for the manipulator is achieved by using an inverse-kinematics controller.**

I. Introduction

A terrestrial mobile manipulator is suited for transporting objects from a place to another while avoiding obstacles and for achieving other tasks such as opening doors, tracking objects with a camera mounted on the manipulator and more. When such a robot traverses uneven terrain then the problem of the robot's tip-over stability becomes accentuated on top of the existing constraints such as joint limits, motor speed-torque limits, singular configurations, and obstacle regions.

The present work addresses the problem of whether the degrees of freedom added to a mobile robotic system through the incorporation of a manipulator can help increase the robot's stability, while satisfying other constraints that were just mentioned.

Most of the past works on the mobile manipulators have been focused on planning and controlling paths on the level surface, while satisfying the aforementioned constraints and guaranteeing the *stability degree* [1], *manipulability* [2] or *task compatibility* [3]. In addition, they assume that the path (or trajectory) for the end-effector of the manipulator is given [4], [5].

In the present work, we focus on generating a path that optimizes the overall tip-over stability (defined as the force-angle stability measure [6]) over a sloped terrain by shifting the center of mass of the manipulator accordingly. This search is performed by using a stochastic optimization method (*Covariance Matrix Adaptation (CMA)* algorithm) [7].

The manipulator employed in the present work has five degrees of freedom, but the degree of freedom related to the gripper is not considered because it does not significantly influence on the location of the center of mass of the manipulator. Hence, the resulting manipulator has four degrees of freedom, and, therefore, it is a redundant system. The redundancy problem is typically resolved either by kinematic control [8], optimal control [9]–[11] or nonlinear optimization method [12]. We resolve the redundancy problem by finding joint angular velocities that minimize the error between the desired task-space velocities and the actual task-space velocities. In this manner, the mobile manipulator can track the two trajectories: one for the base and the other for the center of mass of the arm.

Jae-Yun Jun, Vincent Padois and Faïz Benamar are with:
1. Sorbonne Universités, UPMC Univ Paris 06, UMR 7222, ISIR, F-75005, Paris, France
2. CNRS, UMR 7222, ISIR, F-75005, Paris, France
e-mail: jaeyunjk@gmail.com, padois@isir.upmc.fr, amar@isir.upmc.fr

Fig. 1. A *Cameleon EOD*, a tracked mobile robot from *Eca Robotics* [13]

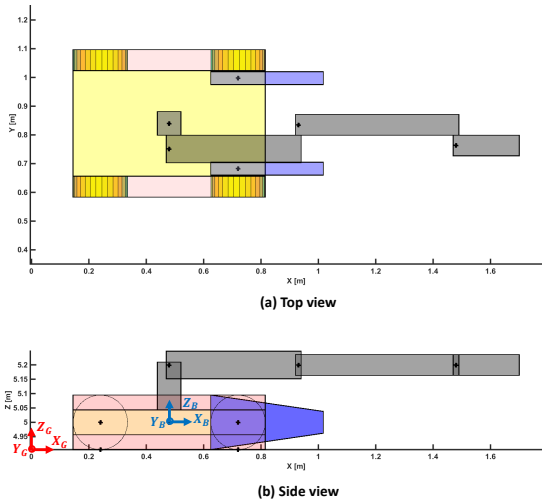

Fig. 2. Tracked mobile robot model: (a) top view, and (b) side view.

The rest of the present work is structured as follows. In Section II, we describe the model for the mobile manipulator employed in the present work, the planning method for the arm configuration for increasing the robot's overall stability over a ramp, and the trajectory tracking for both the base and the arm, where the base is asked to track a circular trajectory on the ramp. In Section III, the results of both the planning for the arm configuration and the trajectory tracking are shown, as well as the improvement achieved by the arm reconfiguration. Finally, in Section IV, we summarize the presented work with some guidance for future work.

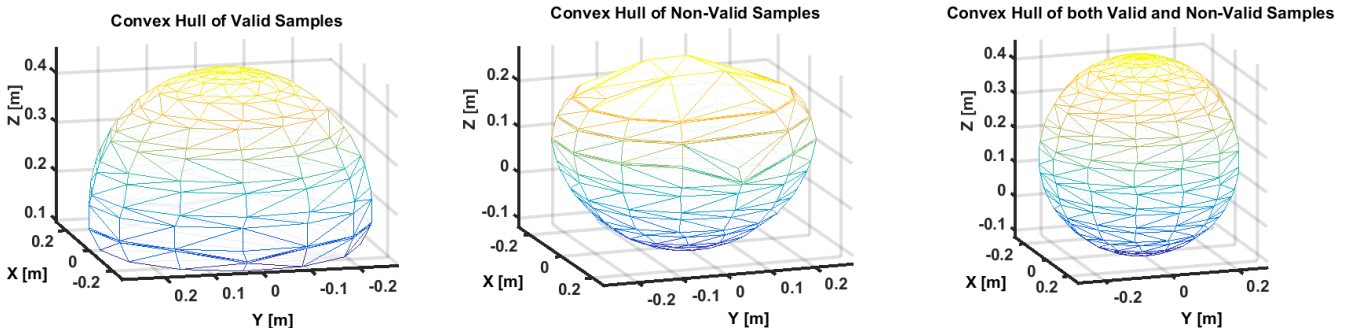

(a) Convex hull for the arm's valid CoMs (b) Convex hull for the arm's non-valid CoMs (c) Convex hull for both valid and non-valid arm's CoMs

Fig. 3. The workspace for the CoM of the manipulator is defined as the subtraction of the convex hull for the non-valid CoMs of the manipulator ((b)) from the convex hull for both the valid and non-valid CoMs of the manipulator ((c)).

II. Methods

A. Description of the robot model

The mobile manipulator considered in the present work is modeled after the robot shown in Fig. 1. The model corresponding to this robot is shown in Fig. 2. The robot base consists of a tracked mobile robot with two tracks and two flippers. The two tracks are actuated with two DC motors, and the flippers are coupled and driven by one DC motor. The flippers are only considered in the present study as collidable bodies, and they are actuated. On the other hand, the manipulator has five degrees of freedom with four links and one gripper. In the present study, the degree of freedom for the gripper is not considered because it does not significantly influence on the location of the center of mass (CoM) of the entire manipulator (Fig. 2). Hence, the manipulator is assumed to have four degrees of freedom.

A coordinate frame is attached to the center of the base, representing the body frame. The arm links are represented using the Denavit Hartenberg's parameters [14]. Hence, a coordinate system is attached to each joint with the purpose to represent the CoM of each link.

The CoM of the manipulator can be expressed as a function of the CoM of each manipulator link as

$$ {}^{G}\mathbf{g}_a = \frac{{}^{G}\mathbf{T}_B \sum_{i=0}^{3} m_i {}^{B}\mathbf{T}_{R_i} {}^{R_i}\mathbf{g}_i}{\sum_{i=0}^{3} m_i}, \tag{1} $$

where ${}^{G}\mathbf{g}_a$ is the CoM of the manipulator in the global frame (see Fig. 2(b)), ${}^{G}\mathbf{T}_B$ is the homogeneous transformation from the body frame ($\{B\}$) to the global frame ($\{G\}$), ${}^{B}\mathbf{T}_{R_i}$ is the homogeneous transformation from the i-th manipulator link frame (R_i) to the body frame, ${}^{R_i}\mathbf{g}_i$ is the CoM of the i-th manipulator link expressed in the i-th manipulator link frame (R_i), and m_i is the mass of the i-th manipulator link.

B. Definition of the workspace for the center of mass of the manipulator in the body frame

The search for the optimal CoM of the manipulator can be efficient if one defines the workspace for the CoM of the manipulator in the body frame in off-line using the brute force method. That is, all possible locations of the manipulator's CoM are identified by considering all possible values for the four joint angles that define the manipulator's configuration with some precision (having the robot platform on a flat surface). Hence, in the definition of the workspace of the manipulator's CoM two types of constraints are taken into account: the joint angle limits for each joint and the self-collision detection. The self collision is detected using the *Gilbert-Johnson-keerthi (GJK)* algorithm [15]. The self collision is checked between all the four links that form the manipulator and the main platform, the two tracks and the two flippers. That is, for all possible values for the four joint angles, the collision between bodies (manipulator links, main-base, tracks and flippers) is checked. If no collision is occurred, then the corresponding CoM of the manipulator is labeled as a valid one. Otherwise, a non-valid label is attributed. This procedure is repeated for all the considered joint-angle values.

This workspace is not convex due to the geometric constraints of the manipulator links and the collision with the base platform (the main body, the two tracks and the two flippers). However, if one can express this space as a combination of convex hulls, then the identification procedure of whether a point is within this workspace can be quickly evaluated. For this reason, first from the clouds of both valid and non-valid CoMs (non-valid due to the collision) a convex hull is formed (Fig. 3(c)). Afterwards, another convex hull is formed from the cloud of non-valid CoMs (Fig. 3(b)). Then, the workspace for the CoM of the manipulator (denoted as $\mathbf{V}$) is defined as the subtraction of the convex hull for the non-valid CoMs of the manipulator from the convex hull for both the valid and non-valid CoMs of the manipulator. This workspace is shown in Fig. 3(a).

C. Relating the tip-over stability to the CoM of the arm

The optimality criterion for searching the desired CoM of the arm employed for the present work is the tip-over stability. In particular, the force-angle stability measure [16] is used. The force-angle stability measure can be computed as the product between the magnitude of the net force and the

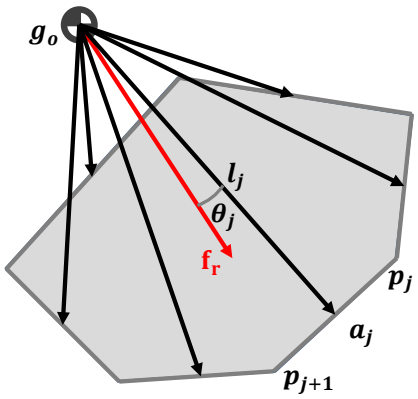

Fig. 4. The robot's tip-over stability can be defined as the force-angle stability measure [16]. The tipover axes ($\mathbf{a}_j$) are the vectors that define the support polygon boundary, and the force-angle stability measure can be computed as the product between the magnitude of the net force and the smallest angle obtained among all the angles formed between the tipover-axis normals ($\mathbf{l_i}$'s) and the net force vector ($\mathbf{f_r}$). The details on the definition of the force-angle stability measure are given in the text.

smallest angle obtained among all the angles formed between the tipover-axis normals ($\mathbf{l_i}$'s) and the net force vector ($\mathbf{f_r}$), where the tipover axes ($\mathbf{a}_j$) are the vectors that define the support polygon boundary. Therefore, the stability measure can be defined as

$$\mu = \min_j (\theta_j) \|\mathbf{f}_r\|, \quad j = \{1, \cdots, n\}, \tag{2}$$

where n is the number of tipover axis of the support polygon, $\mathbf{f_r}$ is the resulting force vector, $\mathbf{a_j}$ is the j-the tipover axis, $\mathbf{l_j}$ is the vector normal to the j-th tip-over axis, and θ_j is the angle formed between $\mathbf{f_r}$ and $\mathbf{l_j}$. See Fig. 4 for clarification.

Therefore, the stability maximization problem can be formulated as

$$\begin{aligned} \max_{\mathbf{g_a}} \quad & \mu(\mathbf{g_a}) \\ \text{s.t.} \quad & \mathbf{g_a} \in \mathbf{V}, \end{aligned} \tag{3}$$

where $\mathbf{g_a}$ is the CoM of the manipulator, and $\mathbf{V}$ is the workspace for the CoM of the manipulator.

On the other hand, one can develop (2) to relate the stability measure to the overall CoM as

$$\theta_j = \sigma_j \cos^{-1}\left(\mathbf{f_r}^{\mathrm{T}} \mathbf{\Phi_j}^{\mathrm{T}} \mathbf{\Phi_j} (\mathbf{p}_{j+1} - \mathbf{g_o})\right), \tag{4}$$

where $\mathbf{\Phi_j} = \left(\mathbf{I} - \hat{\mathbf{a}}_\mathbf{j}\hat{\mathbf{a}}_\mathbf{j}^{\mathrm{T}}\right)$, $\hat{\mathbf{a}}_\mathbf{j} = \mathbf{a}_j / \|\mathbf{a}_j\|$, and

$$\sigma_j = \begin{cases} 1, & \left(\mathbf{\Phi_j} \mathbf{f_r} \times \hat{\mathbf{l}}_\mathbf{j}\right)^{\mathrm{T}} \cdot \hat{\mathbf{a}}_\mathbf{j} > 0, \\ -1, & \text{otherwise.} \end{cases}$$

where $\hat{\mathbf{l}}_\mathbf{j} = \mathbf{l}_j / \|\mathbf{l}_j\|$. Finally, $\mathbf{g_o}$ in (4) can be related to $\mathbf{g_a}$ by

$$\mathbf{g_o} = \frac{m_a \mathbf{g_a} + m_b \mathbf{g_b}}{m_T}, \tag{5}$$

where $\mathbf{g_o}$ is the overall CoM, $\mathbf{g_a}$ is the CoM of the manipulator, $\mathbf{g_b}$ is the CoM of the robot base, $m_T = m_a + m_b$ is the total mass, m_a is the manipulator's mass, and m_b is the robot base's mass.

To validate the stability measure, some nonzero roll value is given to the robot base, and the center of mass of the manipulator is varied by rotating the manipulator's link0 from 0 deg to 360 deg (see Fig. 5(a)). Fig. 5(b) shows that there are two local maxima (among which the one that is close to 2π is the global maximum). The two local maxima roughly correspond to having the manipulator towards the two vertices of the robot side that is lifted. They are not equal because the manipulator is not symmetric due to its links' volumes (geometric constraints).

In addition, we considered eleven robot configurations on a ramp following a circular path as shown in Fig. 6(a). For each robot configuration, the manipulator's link0 is rotated 360 degrees with some precision ($2\pi/100$), and for each sample the corresponding stability measure value is recorded. Notice that the other manipulator links (1,2,3) have zero joint angle, and, hence, the manipulator is stretched all the time while it rotates about the link0's vertical axis. Fig. 6(b) shows these results. Each stability curve presents two local maxima and two local minima. The two local maxima correspond to the manipulator facing to the two corners of the upper face on

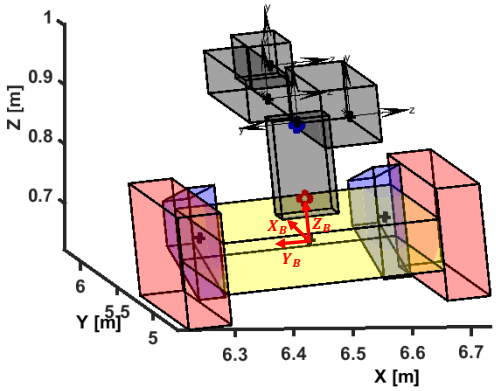

(a) A robot configuration on a ramp

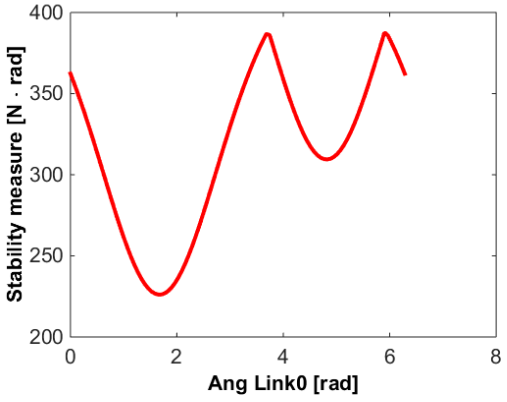

(b) The corresponding stability measure

Fig. 5. Stability measure for 360 degrees of the link 0, while the robot base is located on a ramp with nonzero roll value and zero pitch value.

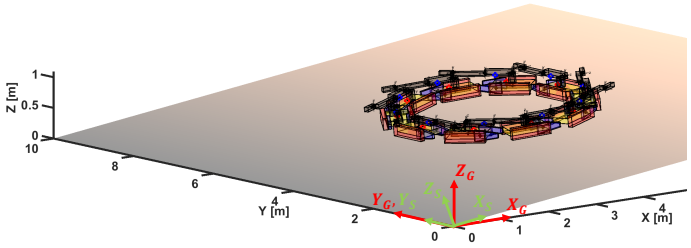

(a) Eleven robot poses on a ramp following a circular path

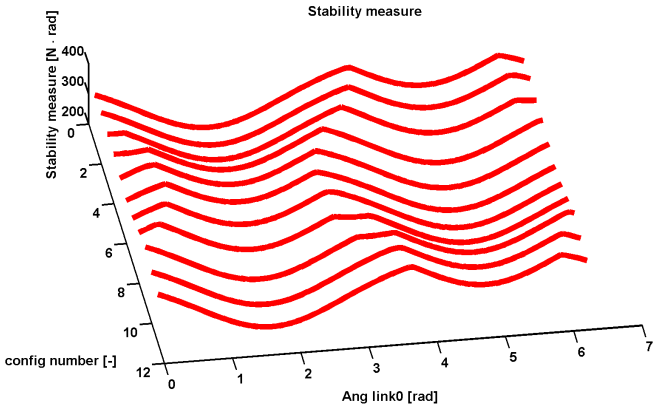

(b) Stability measure values corresponding to the eleven configurations

Fig. 6. Eleven robot configurations are considered on a ramp and following a circular path. For each configuration the manipulator's link0 is rotated 360 degrees with some precision. For each sampling the robot's stability measure is recorded.

the ramp. Among these two maxima, one always has larger stability value because of the asymmetry of the manipulator due to its geometry (see Fig. 5(a)).

D. Search for the optimal location of the overall center of mass

Next, the desired overall CoM is searched as function of the robot platform's pose using a stochastic optimization method known as the *Covariance Matrix Adaptation (CMA)* algorithm) [7] that maximizes the following fitness function

$$\text{fitness} = \omega_1 \frac{\mu}{\mu_{\max}} - \omega_2 \frac{\left(\mathbf{g_o}^{t} - \mathbf{g_o}^{t-1}\right)^2}{\mathrm{d}^2_{\text{workspace}}}, \qquad (6)$$

where $\omega_1 \geq 0$ and $\omega_2 \geq 0$ are the weights satisfying the condition $\omega_1+\omega_2=1$, μ is the stability function introduced in (2), $\mathbf{g_o}^{t}$ is the currently desired CoM of the manipulator, and $\mathbf{g_o}^{t-1}$ is the CoM of the manipulator in the previous time step. The $\mu_{\max}$ is the stability measure corresponding to that of when the robot platform is on a flat surface (with the manipulator folded). Whereas, $\mathrm{d}_{\text{workspace}}$ is the largest distance of the arm's CoM workspace shown in Fig. 3. In this study, we would like to maximize the stability and minimize the motion of the manipulator from the previous time step. During the sampling procedure, if a randomly sampled configuration does not belong to the workspace defined for the CoM, then such a configuration is discarded. As an example, Fig. 7(a) shows an initial set of randomly chosen samples for the arm's CoM with their corresponding arm configurations with the robot base having some nonzero roll angle, and Fig. 7(b) shows the CMA convergence result. That is the arm configuration that corresponds to the arm's CoM that gives the best overall stability.

We do not perform the inverse kinematics to find the joint angles corresponding to the desired CoM of the manipulator in each iteration of the CMA. This is because first it is very expensive to perform the inverse kinematics, and, second, there is no need to perform this task to compute the objective (i.e., fitness) function value associated to each configuration shown in (8).

Because the CMA algorithm might not be able to search for the global optima but be stuck to a local maximum, for each case we considered two sets of initial conditions around the two local minima. Fig. 6(b) indicates that for all the considered cases the manipulator's CoMs correspond to having the link0 joint angle around 2.0 rad and 5.0 rad and the other joint angles being zero. Hence, two initial manipulator CoMs are considered by performing the forward kinematics with the aforementioned joint angle values.

Ten converged manipulator configurations are shown when the mobile manipulator is asked to follow a circular path on a ramp as shown in Fig. 8. For this simulation ω_1=0.9 and ω_2=0.1 are used. The results show that for the first four robot configurations, the manipulator is reconfigured to be on the front right side. Then the manipulator is reconfigured towards

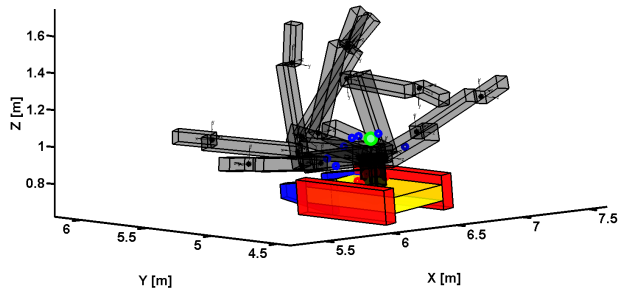

(a) One CMA optimization iteration

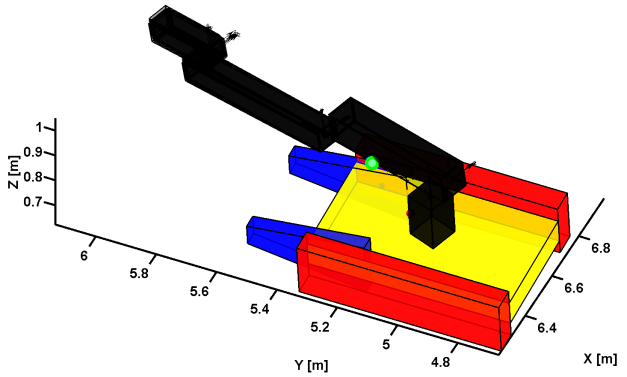

(b) The optimal manipulator's CoM found using the CMA

Fig. 7. A number of arm configurations are considered to compute their arm's CoM and the associated objective function value. Afterwards the mean of the these CoMs is computed.

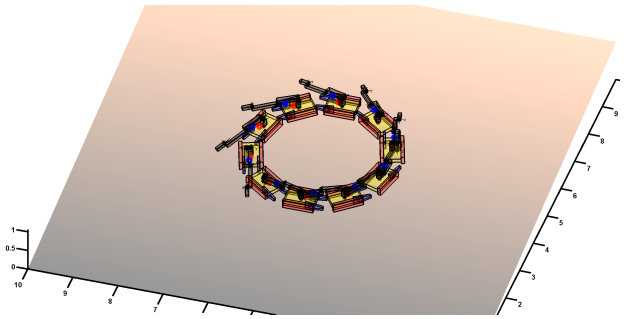

Fig. 8. Converged configurations on a ramp.

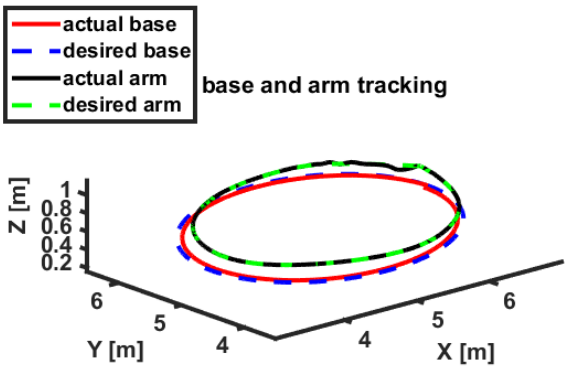

Fig. 9. Desired and actual trajectories for the platform and the arm on the slope.

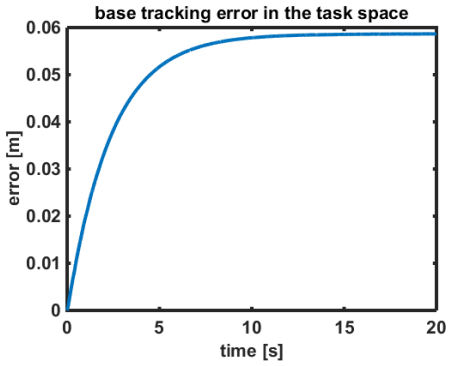

(a) Tracking error for the base

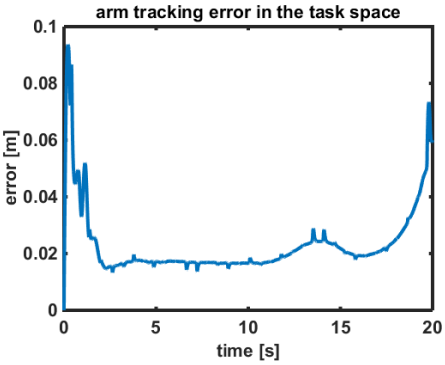

(b) Tracking error for the arm

Fig. 10. Tracking error for both the base and the arm

the front left side during the subsequent four robot base configurations. Finally, the manipulator is again reconfigured to the front right side for the last two configurations. All these reconfigurations show that they are chosen such that the range of the manipulator motion is reduced. Therefore, all these configurations are around one local maximum (regardless whether this corresponds to the global maximum in terms of the stability only). The choice between the left and right is made based on the one that increases the stability.

E. Trajectory tracking

Once the CoM of the manipulator that optimizes (8) is found for each base configuration and a desired path that connects the start and ending configurations is found, then one can control the motion of the manipulator such that its CoM passes through the desired CoM of the manipulator by implementing a controller that satisfies the following optimization problem:

$$\begin{aligned} \min_{\dot{\mathbf{q}}} \quad & \tfrac{1}{2}\|{}^S\dot{\xi}_{\text{des}} - {}^S\mathbf{J}(\mathbf{q})\dot{\mathbf{q}}\|^2_{\omega_A} + \tfrac{1}{2}\|\dot{\mathbf{q}}\|^2_{\omega_B}, \\ \text{s.t.} \quad & \mathbf{q} \le \mathbf{q}_{\text{limit}}, \\ & \dot{\mathbf{q}} \le \dot{\mathbf{q}}_{\text{limit}}, \end{aligned} \tag{7}$$

where ${}^S\dot{\xi}_{\text{des}}$ can be designed as

$${}^S\dot{\xi}_{\text{des}} = K_p\left({}^S\xi_{\text{des}} - {}^S\xi\right). \tag{8}$$

${}^S\xi = [g_{b_x}, g_{b_y}, \gamma, g_{a_x}, g_{a_y}, g_{a_z}]^T$ indicates both the current base configuration and the current arm's CoM described in the Slope Frame (S) (see Fig. 6(a)), $\mathbf{q} = [\theta_l, \theta_r, \theta_0, \theta_1, \theta_2, \theta_3]^T$ indicating the two motor joint angles for the robot base and the four joint angles for the manipulator, $\mathbf{J}(\mathbf{q})$ is the 6×6 Jacobian , $\mathbf{q}_{\text{limit}}$ is 6D joint angle limits, $\dot{\mathbf{q}}_{\text{limit}}$ is 6D joint angular speed limits, $\mathbf{K_p}$ is the 6×6 proportional gain diagonal matrix, ξ_{des} is defined by the desired trajectories for the robot base and the manipulator, and ω_A and ω_B represent the weights for the two additive functions employed in the cost function.

III. Results

Fig. 9 shows the tracking of both the trajectory for the control point of the base and the trajectory for the CoM of the arm as the robot traverses on the slope.

In fact, Fig. 10(a) and Fig. 10(b) show a closer look on the tracking performance using the controller described in the previous section. The tracking errors for both the base and the arm are bounded.

Fig. 11 shows the joint angular velocities for both the base and the arm. In the optimization problem shown in the previous section, the joint angular velocities are limited by 4π rad/s. Fig. 11(a) shows that the saturation of the joint angular velocities during the initial stage of the simulation. In general, the first arm link has larger values of angular velocity because the desired trajectory for the center of mass of the arm mainly moves parallel to the slope plane with small changes along the direction normal to this plane.

On the other hand, Fig. 11(b) shows that the joint angular velocities for the base quickly raise to reach the desired velocities. One can also see that the values of the angular

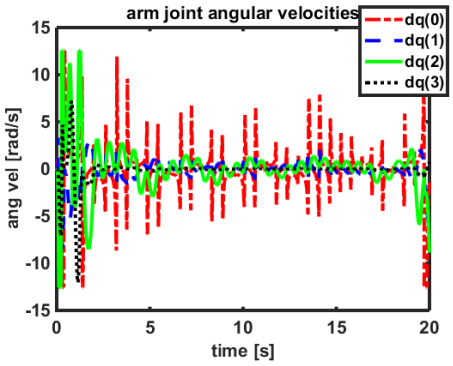

(a) Angular velocities of the arm joints

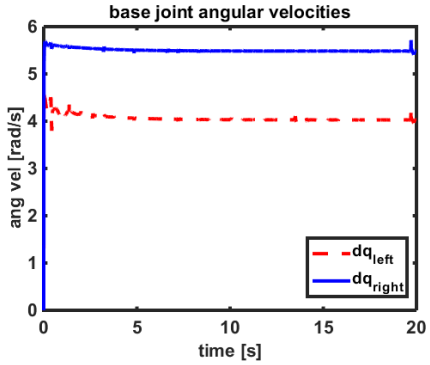

(b) Angular velocities of the base joints

Fig. 11. Angular velocities for the arm joints and the base joints

velocity of the right side joint are always larger than those of the left side joint. This result is because the robot is asked to track the circular trajectory counterclockwisely, and, therefore, the left side of the robot is the inner side as the robot tracks the desired trajectory.

Finally, Fig. 12 shows the force-angle stability measure as the mobile manipulator tracks the trajectories. In the future, we will compare these results to the stability measures achieved with different robot configurations.

Finally, we compare the stability achieved as the robot tracks the trajectories shown in Fig. 9 by reconfiguring its arm to the stability result obtained by removing the arm from the robot base. As the comparison results demonstrate, a clear stability improvement can be achieved by the arm reconfiguration.

IV. Conclusion and Future Work

We propose in this paper a method for motion generation and control of a mobile manipulator intended to navigate on rough terrain, which can be considered to be as set of slopes. The arm motion generation is defined by optimizing the stability margin of the overall system. The inverse kinematics-based controller ensures both tracking of the mobile base and the arm's center of mass. The proposed approach is validated in simulation on a slopping ground, and, in the future, this method will be generalized to other types of uneven terrains.

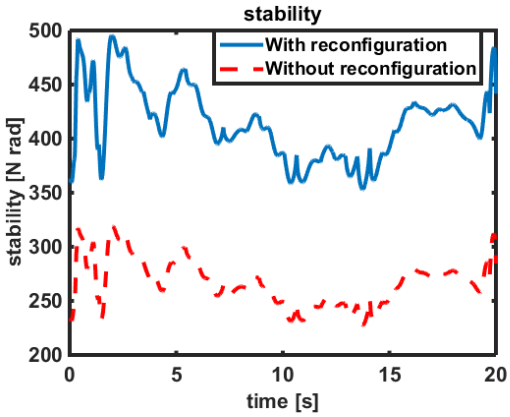

Fig. 12. The tip-over stability measure while the mobile manipulator tracks the trajectories.

References

[1] S. Sugano, Q. Huang, and I. Kato, "Stability criteria in controlling mobile robotic systems," in *1993 International Conference on Intelligent Robots and Systems. Part 2 (of 3), July 26, 1993 - July 30, 1993*. Yokohama, Jap: Publ by IEEE, 1993, pp. 832–838.

[2] T. Yoshikawa, *Foundations of robotics: analysis and control*. Cambridge, Massachusetts: The MIT Press, 1990.

[3] S. L. Chiu, "Task compatibility of manipulator postures," *The International Journal of Robotics Research*, vol. 7, no. 5, pp. 13–21, 1988.

[4] A. Mohri, S. Furuno, and M. Yamamoto, "Trajectory planning of mobile manipulator with end-effector's specified path," in *Proc. of IEEE/RSJ International Conference on Intelligent Robots and Systems*, 2001.

[5] G. Oriolo and C. Mongillo, "Motion planning for mobile manipulators along given end-effector paths," in *Proc. of IEEE International Conference on Robotics and Automation*, 2005.

[6] E. Papadopoulos and D. A. Rey, "Force-angle measure of tipover stability margin for mobile manipulators," *Vehicle System Dynamics*, vol. 33, no. 1, pp. 29–48, 2000.

[7] N. Hansen and A. Ostermeier, "Adapting arbitrary normal mutation distributions in evolution strategies: The covariance matrix adaptation," in *Proc. of IEEE International Conference on Evolutionary Computation*, 1996.

[8] B. Siciliano, "Kinematic control of redundant robot manipulators: a tutorial," *Journal of intelligent and robotic systems*, vol. 3, pp. 201–212, 1990.

[9] D. P. Martin, J. Baillieul, and J. M. Hollerbach, "Resolution of kinematic redundancy using optimization techniques," *IEEE Transactions on Robotics and Automation*, vol. 5, no. 4, pp. 529–533, 1989.

[10] W. Miksch and D. Schroeder, "Performance-functional based controller design for a mobile manipulator," in *Proc. of IEEE International Conference on Robotics and Automation*, 1992.

[11] C.-C. Wang and V. Kumar, "Velocity control of mobile manipulators," in *Proc. IEEE International Conference on Robotics and Automation*, 1993.

[12] F. G. Pin, J.-C. Culioli, and D. B. Reister, "Using minimax approaches to plan optimal task commutation configurations for combined mobile platform-manipulator systems," *IEEE Transactions on Robotics and Automation*, vol. 10, no. 1, pp. 44–54, 1994.

[13] Cameleon EOD, Eca Robotics: http://www.eca-robotics.com/en/robotic-vehicle/robotics-terrestrial-unmanned-ground-vehicles-(ugv)-cameleon-eod-lightweight-eod-ugv/22.htm.

[14] R. Hartenberg and J. Denavit, *Kinematic synthesis of linkages*. McGraw-Hill, 1965.

[15] E. G. Gilbert, D. W. Johnson, and S. Keerthi, "Fast procedure for computing the distance between complex objects in three-dimensional space," *IEEE Journal of Robotics and Automation*, vol. 4, no. 2, pp. 193–203, 1988.

[16] E. Papadopoulos and D. Rey, "A new measure of tipover stability margin for mobile manipulators," in *Proc. IEEE International Conference on Robotics and Automation*, vol. vol.4, Minneapolis, MN, USA, 1996, pp. 3111–16.